

Stable dilute supersolid of two-dimensional dipolar bosons

Zhen-Kai Lu,¹ Yun Li,² D. S. Petrov,³ and G. V. Shlyapnikov^{3,4,5,6}

¹*Max-Planck-Institut für Quantenoptik, Hans-Kopfermann-Straße 1, 85748 Garching, Germany*

²*Centre for Quantum and Optical Science, Swinburne University of Technology, Melbourne, Victoria, 3122, Australia*

³*Université Paris-Sud, CNRS, LPTMS, UMR8626, Orsay, F-91405, France*

⁴*Van der Waals-Zeeman Institute, University of Amsterdam, Science Park 904, 1098 XH Amsterdam, The Netherlands*

⁵*Russian Quantum Center, Novaya street 100, Skolkovo, Moscow region 143025, Russia*

⁶*Wuhan Institute of Physics and Mathematics, Chinese Academy of Sciences, Wuhan 430071, China*
(Dated: June 9, 2015)

We consider two-dimensional bosonic dipoles oriented perpendicularly to the plane. On top of the usual two-body contact and long-range dipolar interactions we add a contact three-body repulsion as expected, in particular, for dipoles in the bilayer geometry with tunneling. The three-body repulsion is crucial for stabilizing the system, and we show that our model allows for stable continuous space supersolid states in the dilute regime and calculate the zero-temperature phase diagram.

PACS numbers: 03.75.Hh, 05.30.Rt, 67.80.K-, 67.85.-d

Recent advances in the field of cold polar molecules [1, 2] and magnetic atoms [3, 4] interacting via long-range dipole-dipole forces make it realistic to create novel many-body quantum states in these systems. For polar molecules, ultracold chemical reactions observed at JILA [5, 6] and leading to a rapid decay of the system can be suppressed by tightly confining the molecules to a (quasi)two-dimensional (2D) geometry, orienting the dipoles perpendicularly to the plane of their translational motion, and thus inducing a strong intermolecular repulsion [7–9]. Therefore, 2D geometries are intensively discussed in the context of ultracold dipolar gases [10, 11], together with possible experiments with non-reactive molecules, such as NaK [12, 13] and RbCs [14, 15].

The studies of ultracold dipolar gases may open perspectives for the observation of supersolidity. This remarkable quantum phenomenon combines superfluidity with a crystalline order [16, 17] (see [18] for review). It is still under debate as to what extent experimental results in solid helium prove the existence of this conceptually important phase [19]. On the other hand, supersolidity is rather well understood theoretically for soft-core two-body potentials [18, 20–24] which can be realized, for example, in Rydberg-dressed atomic gases. However, such supersolids require a dense regime with at least several particles within the interaction range, which can be difficult to achieve. The same holds for supersolids discussed for 2D dipolar Bose gases [25] near the gas-solid phase transition [26, 27]. It is thus an open question whether supersolids can exist in the dilute regime. The creation of such supersolids, especially if they are tunable regarding the lattice period, will allow for studies of non-conventional superfluid properties of supersolids and other aspects of supersolidity. Dilute 2D dipolar bosons may show the (helium-like) roton-maxon structure of the spectrum by fine-tuning the short-range part of the interaction potential and can be made unstable with respect to periodic modulations of the order parameter (roton

instability) [28]. However, instead of forming a supersolid state when approaching such an instability, the gas collapses [29, 30].

In this Letter we predict a stable supersolid state in a dilute two-dimensional dipolar system. In contrast to the earlier proposed soft-core supersolids, where the lattice period is of the order of the core radius, in our case it is tunable by varying the density and the dipole moment. In addition to the contact two-body term (g_2) and the dipole-dipole long-range tail characterized by the dipole moment d , we include a contact repulsive three-body term (g_3) which may prevent the collapse. Three-body forces are ubiquitous and arise naturally in effective field theories when one integrates out some of the high-energy degrees of freedom in the system [31]. In particular, our model can be realized for dipoles in the bilayer geometry with interlayer tunneling [32]. Tracing out the degree of freedom associated with the layer index one obtains an effective single-layer model in which g_2 and g_3 can be independently controlled by tuning the interlayer tunneling amplitude. Here we work out the phase diagram of this model and identify stable uniform and supersolid states.

The Hamiltonian of the system reads

$$\mathcal{H} = - \int d^2r \hat{\psi}^\dagger(\mathbf{r}) \frac{\hbar^2 \nabla^2}{2m} \hat{\psi}(\mathbf{r}) + \mathcal{H}_2 + \frac{g_3}{6} \int d^2r \hat{\psi}^\dagger(\mathbf{r}) \hat{\psi}^\dagger(\mathbf{r}) \hat{\psi}^\dagger(\mathbf{r}) \hat{\psi}(\mathbf{r}) \hat{\psi}(\mathbf{r}) \hat{\psi}(\mathbf{r}), \quad (1)$$

where $\hat{\psi}(\mathbf{r})$ is the bosonic field operator, m is the particle mass, and the normalization volume is set equal to unity. The first term in Eq. (1) corresponds to the kinetic energy, the third one to the contact three-body repulsion ($g_3 > 0$), and the two-body interaction Hamiltonian \mathcal{H}_2 at low energies can be substituted by an effective momentum-dependent (pseudo)potential (see, e.g., [33])

$$\tilde{V}(\mathbf{k}, \mathbf{k}') = \tilde{V}(|\mathbf{k} - \mathbf{k}'|) = g_2 - 2\pi d^2 |\mathbf{k} - \mathbf{k}'|, \quad (2)$$

where \mathbf{k} and \mathbf{k}' are the incoming and outgoing relative momenta, g_2 is the contact term which depends on the short-range details of the two-body potential, and the momentum-dependent part corresponds to the long-range dipolar tail for dipoles oriented perpendicularly to the plane of their translational motion. We thus have

$$\mathcal{H}_2 = \frac{1}{2} \int d^2r d^2r' \hat{\psi}^\dagger(\mathbf{r}) \hat{\psi}^\dagger(\mathbf{r}') \sum_{\mathbf{q}} \tilde{V}(\mathbf{q}) e^{i\mathbf{q}(\mathbf{r}'-\mathbf{r})} \hat{\psi}(\mathbf{r}) \hat{\psi}(\mathbf{r}'). \quad (3)$$

The onset of supersolidity is frequently associated with the presence of a low-lying roton minimum in the excitation spectrum [21, 34, 35]. In our case the standard Bogoliubov approach for a uniform Bose condensate of density n gives the excitation spectrum

$$\epsilon(k) = \sqrt{E_k^2 + 2E_k(g_2n + g_3n^2 - 2\pi n d^2 k)}, \quad (4)$$

where $E_k = \hbar^2 k^2 / 2m$, and we assume that $(g_2 + g_3n) > 0$. The validity conditions for the mean-field approach read

$$nr_*^2 \ll 1; \quad m(g_2 + g_3n)/\hbar^2 \ll 1, \quad (5)$$

where $r_* = md^2/\hbar^2$ is a characteristic range of the dipole-dipole interaction. The structure of the spectrum is characterized by a dimensionless parameter β given by

$$\beta = \gamma / (1 + g_2/g_3n); \quad \gamma = 4\pi^2 \hbar^2 r_*^2 / mg_3. \quad (6)$$

The excitation energy $\epsilon(k)$ shows a roton-maxon structure (local maximum and minimum at finite k) for β in the interval $8/9 < \beta < 1$, and at $\beta = 1$ the roton minimum touches zero. For $\beta > 1$ the excitation energies become imaginary, and the uniform superfluid (U) is dynamically unstable and is no longer the ground state.

A promising candidate for the new ground state is a supersolid state in which the condensate wavefunction is a superposition of a constant term and a lattice-type function of coordinates [16, 17, 21, 34]. We considered various lattice structures and found that the ground state can be either a triangular lattice supersolid (T) or a stripe supersolid (S) [36]. For T, the lattice is built up on three vectors in the x, y plane of the translational motion, with the angle of $2\pi/3$ between each pair: $\mathbf{k}_1 = (k, 0)$, $\mathbf{k}_2 = (-k/2, \sqrt{3}k/2)$, and $\mathbf{k}_3 = (-k/2, -\sqrt{3}k/2)$, while for the S phase the density modulation depends only on one wave vector $\mathbf{k} = (k, 0)$.

The variational ansatz for the condensate wavefunction of the T phase then takes the form:

$$\psi_T(\mathbf{r}) = \sqrt{n} \left(\cos \theta + \sqrt{2/3} \sin \theta e^{i\Phi} \sum_i \cos \mathbf{k}_i \mathbf{r} \right), \quad (7)$$

and for the S phase we have:

$$\psi_S(\mathbf{r}) = \sqrt{n} \left(\cos \theta + \sqrt{2} \sin \theta e^{i\Phi} \cos kx \right), \quad (8)$$

which satisfies the normalization condition $\int d\mathbf{r} |\psi_{T(S)}(\mathbf{r})|^2 = n$, with n being the mean density. The variational parameters of the wavefunctions are θ , Φ , and k . Density modulations appear at $\theta \neq 0$, and thus θ is the order parameter which exhibits the U to supersolid transition. We have checked that the lowest energy always corresponds to $\Phi = 0$ and for brevity we omit this parameter.

For obtaining the energy functionals of the T and S states, we replace the field operators in Eqs. (1) and (3) with $\psi_T(\mathbf{r})$ and with $\psi_S(\mathbf{r})$, respectively. This yields

$$\mathcal{E}_i = [E_k n - 4\pi n^2 d^2 k \mathcal{D}_i(\theta)] \sin^2 \theta + g_2 n^2 \mathcal{C}_i(\theta) + g_3 n^3 \mathcal{T}_i(\theta), \quad (9)$$

where the symbol i stands for T and S, and the functions $\mathcal{D}_{T(S)}(\theta)$, $\mathcal{C}_{T(S)}(\theta)$, and $\mathcal{T}_{T(S)}(\theta)$ are related to the two-body dipole-dipole, two-body contact, and three-body contact interactions, respectively [36].

By minimizing Eq. (9) with respect to k we obtain

$$\mathcal{E}_i(k_{mi}) = g_2 n^2 \mathcal{C}_i(\theta) + g_3 n^3 (\mathcal{T}_i(\theta) - 2\gamma \sin^2 \theta \mathcal{D}_i^2(\theta)), \quad (10)$$

where $k_{mi} = 4\pi n r_* \mathcal{D}_i(\theta)$. In the dilute limit of Eq.(5) the particle number per unit modulation volume is $n(2\pi/k_{mi})^2 \sim 1/nr_*^2 \gg 1$, which justifies the mean-field approach.

The energy functional $\mathcal{E}_{T(S)}$ can be expanded in powers of θ . The zero-order term $\mathcal{E}(\theta = 0) = g_2 n^2 / 2 + g_3 n^3 / 6$ gives the energy density of the uniform state. The expansion of \mathcal{E}_T contains terms $\propto \theta^3$ [36], which is a consequence of the fact that the vectors \mathbf{k}_1 , \mathbf{k}_2 , and \mathbf{k}_3 form a closed triangle (“triad”, $\mathbf{k}_1 + \mathbf{k}_2 + \mathbf{k}_3 = 0$) [17]. In contrast, the expansion of \mathcal{E}_S contains only even powers of θ . According to the Ginzburg-Landau theory [37, 38], the U-supersolid transition should occur to the T phase and it is expected to be first order, so that θ jumps from 0 to a finite value. However, deeply in the supersolid regime the states with different structures are energetically competing and, in particular, the stripe phase can become the ground state of the system.

First-order transitions are convenient to analyse in the grand-canonical picture. We obtain the phase diagram by variationally minimizing the grand potential $\Omega = \mathcal{E}_{T(S)} - \mu n$ with respect to θ and n for given values of the chemical potential μ and the interaction parameters g_2 , g_3 and d . We have checked the phase diagram by employing the full numerical minimization of the grand potential density, which is equivalent to solving the corresponding Gross-Pitaevskii (GP) equation [36].

First, let us consider $g_2 = 0$. In this case the energy functional \mathcal{E} only contains terms $\propto n^3$, and the phase diagram is determined by a single dimensionless parameter γ defined in Eq. (6). The U to T transition occurs before the roton minimum touches zero (for $g_2 = 0$ we have $\beta = \gamma$), namely at $\gamma_0 \simeq 0.99$, where θ jumps from 0 to 0.0946. The inverse compressibility $\kappa^{-1} = \partial\mu/\partial n = 6\mathcal{E}/n^2$ is positive for γ smaller than

approximately 1.4, indicating the existence of a stable supersolid state. However, our numerics predicts the collapse instability at about $\gamma_c \approx 0.88$ and indicates that for lower values of γ the ground state is a uniform superfluid. The discrepancy between the numerics and variational ansatz comes from the fact that the latter does not take into account higher order momentum harmonics.

For $g_2 \neq 0$, we turn to the rescaled dimensionless density $\tilde{n} = ng_3/|g_2|$, chemical potential $\tilde{\mu} = \mu g_3/g_2^2$, and grand potential $\tilde{\Omega}_{T(S)} = (g_3^2/|g_2|^3)\Omega_{T(S)} = \tilde{\mathcal{E}}_{T(S)} - \tilde{\mu}\tilde{n}$. The rescaled energy functional is given by

$$\tilde{\mathcal{E}}_i = [\mathcal{T}_i(\theta) - 2\gamma \sin^2 \theta \mathcal{D}_i^2(\theta)]\tilde{n}^3 + \text{sgn}(g_2)\tilde{n}^2 \mathcal{C}_i(\theta). \quad (11)$$

The phase diagram can be presented in the parameter space $(\tilde{\mu}, \gamma)$ and the phases are characterized by $\theta \in [-\pi/2, \pi/2]$ and \tilde{n} . One can easily see that in the high-density regime $\tilde{\Omega}_{T(S)}$ is dominated by the term $[\mathcal{T}_{T(S)}(\theta) - 2\gamma \sin^2 \theta \mathcal{D}_{T(S)}^2(\theta)]\tilde{n}^3$, whereas the two-body contact interaction, i.e., the term containing $\mathcal{C}_{T(S)}(\theta)$, becomes irrelevant. In this case the T phase has a lower $\tilde{\Omega}$ than the S phase, and we obtain the same stability condition as in the case of $g_2 = 0$. Numerically we find that the phase diagram for $g_2 > 0$ contains only a stable U state at $\gamma < \gamma_c$ and the region of collapse for $\gamma > \gamma_c$.

The situation is quite different for $g_2 < 0$. The phase diagram is shown in Fig. 1 where all continuous curves correspond to the variational results and all symbols to the exact numerical solution of the GP equation. Let us first discuss the variational results. The dashed curves mark the U- $T_{\theta < 0}$ and U- $T_{\theta > 0}$ transitions, which occur for $\tilde{\mu} < 3/2$ and $\tilde{\mu} > 3/2$, respectively. These are first order transitions which weaken on approaching the point $\tilde{\mu} = 3/2$, $\gamma = 2/3$ (black dot). The same holds for the dotted curves, which correspond to the transitions from the T phases to the S phase. The black dot thus stands as a four-critical point and it is the only place in the phase diagram where the transitions are second order and occur when the roton minimum touches zero. In this case the grand potential $\tilde{\Omega} = \text{const} + O(\theta^4)$, i.e., the terms $\propto \theta^2$ and $\propto \theta^3$ are absent.

The region on the left of the black solid curve in Fig. 1 is the vacuum state: $\tilde{n} = 0$, $\Omega = 0$. Directly on the curve, vacuum can coexist with matter which has a finite density and zero pressure. We thus are dealing with a self-trapped droplet state [40]. With increasing γ , the vacuum curve eventually bends towards negative $\tilde{\mu}$ and tends to the variational collapse line $\gamma \approx 1.4$ (not shown).

By solving the GP equation numerically we observe that the overall structure of the phase diagram is well captured by the variational ansätze (7) and (8). Close to the four-critical point the agreement is quantitative, which is generally expected in the regions where $\theta \ll 1$. Far from this point we see that the exact collapse line moves to $\gamma \approx 0.88$ (crosses in Fig. 1) and the vacuum curve (empty orange circles) bends towards negative $\tilde{\mu}$

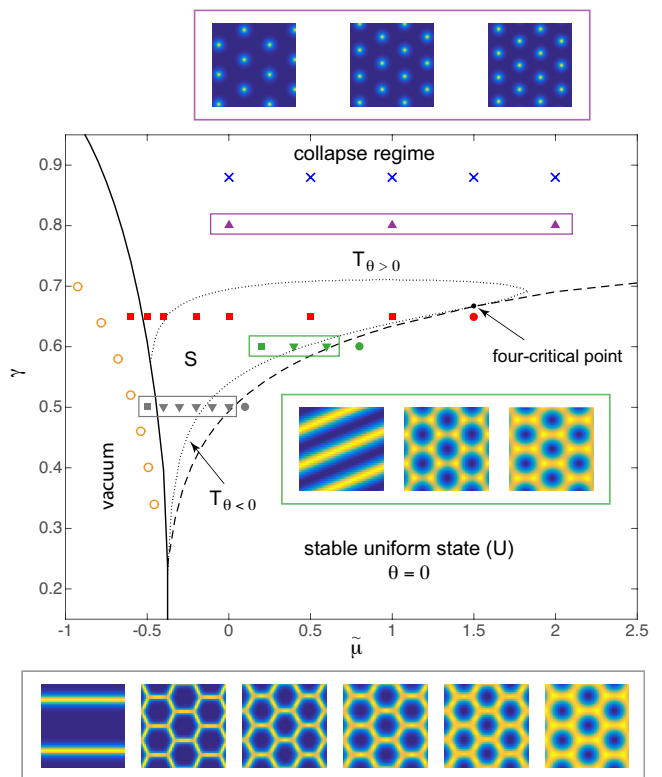


Figure 1. (color online) Phase diagram for $g_2 < 0$. Continuous curves correspond to transitions between different phases obtained from the variational ansätze (7) and (8). Increasing γ one passes the U-T transition (dashed), then T-S (lower dotted curve), and S-T (upper dotted curve). To the left of the solid black curve the ground state of the system is vacuum. The black dot is the four-critical point for the U, S, and two T phases. The symbols indicate our numerical results: the filled circles are inside the U phase, the downward and upward pointing triangles are inside the $T_{\theta < 0}$ and $T_{\theta > 0}$ phases, respectively, and squares are in the stripe phase. The empty circles are on the vacuum-stripe line and crosses are at the collapse instability border. The color-coded pictures show density profiles corresponding to the symbols in the phase diagram put in frames: the upper set (violet frame) contains three points of the $T_{\theta > 0}$ phase at $\gamma = 0.8$, the middle set (green frame) shows one point in the S phase and two points in the hexagonal $T_{\theta < 0}$ phase at $\gamma = 0.6$, and the lower set (grey frame) corresponds to the six points at $\gamma = 0.5$.

faster than its variational version. The rest of the symbols in Fig. 1 are inside the U phase (filled circles), $T_{\theta < 0}$ phase (down triangles), $T_{\theta > 0}$ phase (up triangles), and S phase (squares). We see that the actual U- $T_{\theta < 0}$ phase boundary is well described by the variational method, but one can notice a move of the S phase upwards and towards negative $\tilde{\mu}$. In fact, the vacuum-S- $T_{\theta > 0}$ tri-critical point moves to $\tilde{\mu} \approx -1.27$, $\gamma = 0.78$ (outside of the plot).

In Fig. 1 we also show density profiles corresponding to the points enclosed by rectangular frames in the phase diagram. The blue and yellow colors stand for minima

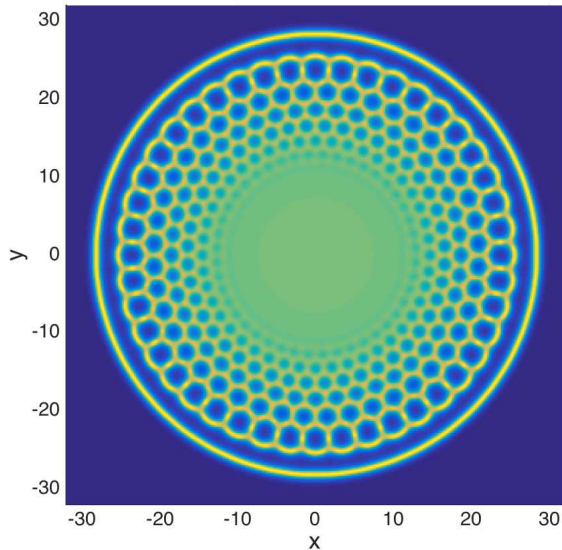


Figure 2. (color online) The density profile for a harmonically trapped gas with $\tilde{\mu} = 0.6$, $\gamma = 0.575$, and trapping frequency $\tilde{\omega} = 0.05$. The coordinates x, y are in units of $\sqrt{\hbar^2 g_3 / m g_2^2}$.

and maxima of the density. Without this rescaling the contrast, for instance, in the lowest rightmost picture would be very weak. However, one can clearly distinguish smooth density profiles, which can be described by a few harmonics in the spirit of Eqs. (7) and (8), and sharper profiles (as one moves further away from the four-critical point) requiring more harmonics or a different ansatz. The spatial coordinates have also been rescaled (except for the upper set in the violet frame) because the wave vector k_m changes very strongly from point to point.

To the right of the vacuum curve (empty circles in Fig. 1) the pressure is $P = -\Omega > 0$ and, therefore, this region of the phase diagram requires an external trapping. In Fig. 2 we present the exact GP result for an isotropically trapped gas with $g_2 < 0$, $\gamma = 0.575$, the global chemical potential $\tilde{\mu} = 0.6$, and trap frequency $\tilde{\omega} = 0.05$ (in units of $g_2^2 / \hbar g_3$). The result is consistent with the local density approximation in which moving from the trap center towards its edge is equivalent to the trajectory along a horizontal line in Fig. 1 determined by the local chemical potential $\mu(r) = \mu - m\omega^2 r^2 / 2$. In Fig. 2 one can clearly distinguish the U phase in the trap center, the transition to the $T_{\theta < 0}$ phase, and eventually to the S phase. As the local chemical potential decreases, the contrast and the period of the density modulation increase, which is consistent with the free space results.

We should point out that first-order transitions involving density jumps are forbidden in 2D systems with dipolar interaction tails. The reason is that the surface tension in between two such phases can have a negative contribution which logarithmically diverges with the length

of the interface and can thus overcome the positive local scale-independent contribution [41] (see also [18]). This means that the first-order transition curves that we describe here become (narrow) regions of intermediate “microemulsion” phases [41]. It is argued [18, 42] that the observation of these phases requires exponentially large system sizes which are likely much larger than the size of a typical ultracold sample. Nevertheless, we note that already the simplest vacuum-U interface that we predict in our dilute weakly-interacting system should be a good candidate for studying these interfacial effects. However, we leave this subject for future work.

In conclusion, we have found that a dilute 2D dipolar Bose gas can reside in a variety of supersolid phases stabilized by three-body repulsion. Our results represent a starting point for the analysis of collective modes of homogeneous, trapped or self-trapped supersolids. The developed approach can also be employed in the studies of novel vortex and soliton structures, and in the search for translationally nonperiodic phases, in particular density-disordered superfluid (superglass) phases. Promising candidates for the creation of such dipolar Bose gases are (nonreactive) polar molecules in the bilayer geometry with interlayer tunneling. At 2D densities $n \sim 10^8 \text{ cm}^{-2}$, for the dipole moment $d \sim 0.5 \text{ D}$ one has $r_* \sim 200 \text{ nm}$ and $nr_*^2 \ll 1$. Then g_3 can be made such [32] that $\gamma \sim 1$ and one may cover the whole range of parameters in the phase diagram of Fig. 1. Finally, our results have implications for magnetic atoms such as erbium or dysprosium, which are necessarily dilute due to their small r_* . However, a mechanism for generating a sufficiently strong three-body repulsion in such gases has yet to be discussed.

We acknowledge support from IFRAF and from the Dutch Foundation FOM. The research leading to these results has received funding from the European Research Council under European Community’s Seventh Framework Programme (FR7/2007-2013 Grant Agreement no.341197). LY acknowledges the support from the ARC Discovery Projects (Grant Nos DE150101636 and DP140103231).

-
- [1] K.-K. Ni, S. Ospelkaus, M.H.G. de Miranda, A. Pe’er, B. Neyenhuis, J.J. Zirbel, S. Kotochigova, P.S. Julienne, D.S. Jin and J. Ye, *Science* **322**, 231(2008).
 - [2] See for review: L.D. Carr, D. DeMille, R.V. Krems, and J. Ye, *New Journal of Physics* **11**, 055049 (2009).
 - [3] M. Lu, N.Q. Burdick, S.H. Youn, and B.L. Lev, *Phys. Rev. Lett.* **107**, 190401 (2011).
 - [4] K. Aikawa, A. Frisch, M. Mark, S. Baier, A. Rietzler, R. Grimm, and F. Ferlaino, *Phys. Rev. Lett.* **108**, 210401 (2012).
 - [5] S. Ospelkaus, K.-K. Ni, D. Wang, M.H.G. de Miranda, B. Neyenhuis, G. Quemener, P. S. Julienne, J. L. Bohn, D. S. Jin, and J. Ye, *Science* **327**, 853 (2010).

- [6] K.-K. Ni, S. Ospelkaus, D. Wang, G. Quéméner, B. Neyenhuis, M.H.G. de Miranda, J.L. Bohn, J. Ye, and D.S. Jin, *Nature* **464**, 1324 (2010).
- [7] G. Quéméner and J. L. Bohn, *Phys. Rev. A* **81**, 060701(2010).
- [8] A. Micheli, Z. Idziaszek, G. Pupillo, M. A. Baranov, P. Zoller, and P. S. Julienne, *Phys. Rev. Lett.* **105**, 073202 (2010).
- [9] M.H.G. de Miranda, A. Chotia, B. Neyenhuis, D. Wang, G. Quemener, S. Ospelkaus, J.L. Bohn, J. Ye, and D.S. Jin, *Nature Phys.* **7**, 502 (2011).
- [10] M.A. Baranov, *Physics Reports* **464**, 71 (2008).
- [11] M.A. Baranov, M. Dalmonte, G. Pupillo, and P. Zoller, *Chemical Reviews* **112**, 5012 (2012).
- [12] C.-H. Wu, J. W. Park, P. Ahmadi, S. Will, M. W. Zwierlein, *Phys. Rev. Lett.* **109**, 085301 (2012).
- [13] J. W. Park, S. A. Will, M. W. Zwierlein, *Phys. Rev. Lett.* **114**, 205302 (2015).
- [14] T. Takekoshi, L. Reichsollner, A. Schindewolf, J. M. Hutson, C. Ruth Le Sueur, O. Dulieu, F. Ferlaino, R. Grimm, and H.-C. Nägerl, *Phys. Rev. Lett.* **113**, 205301 (2014).
- [15] P. K. Molony, P. D. Gregory, Z. Ji, B. Lu, M. P. Köppinger, C. R. Le Sueur, C. L. Blackley, J. M. Hutson, S. L. Cornish, *Phys. Rev. Lett.* **113**, 255301 (2014).
- [16] E. P. Gross, *Phys. Rev.* **106**, 161 (1957); *Ann. Phys.* **4**, 57 (1958).
- [17] D. A. Kirzhnits and Yu. A. Nepomnyashchii, *Sov. Phys. JETP* **32**, 1191 (1971).
- [18] A. B. Kuklov, N. V. Prokof'ev, and B. V. Svistunov, *Physics* **4** 109 (2011); M. Boninsegni and N. V. Prokof'ev, *Rev. Mod. Phys.* **84**, 759 (2012).
- [19] S. Balibar, *Nature (London)* **464**, 176 (2010).
- [20] Here we focus on continuous space supersolids.
- [21] Y. Pomeau and S. Rica, *Phys. Rev. Lett.* **72**, 2426 (1994).
- [22] N. Henkel, R. Nath, and T. Pohl, *Phys. Rev. Lett.* **104**, 195302 (2010).
- [23] F. Cinti, P. Jain, M. Boninsegni, A. Micheli, P. Zoller, and G. Pupillo, *Phys. Rev. Lett.* **105**, 135301 (2010).
- [24] S. Saccani, S. Moroni, and M. Boninsegni, *Phys. Rev. B* **83**, 092506 (2011).
- [25] I.L. Kurbakov, Yu.E. Lozovik, G.E. Astrakharchik, and J. Boronat, *Phys. Rev. B* **82**, 014508 (2010).
- [26] H.P. Buchler, E. Demler, M. Lukin, A. Micheli, N. Prokof'ev, G. Pupillo, and P. Zoller, *Phys. Rev. Lett.* **98**, 060404 (2007).
- [27] G. E. Astrakharchik, J. Boronat, I. L. Kurbakov, and Yu. E. Lozovik, *Phys. Rev. Lett.* **98**, 060405 (2007).
- [28] L. Santos, G.V. Shlyapnikov, and M. Lewenstein, *Phys. Rev. Lett.* **90**, 250403 (2003).
- [29] G.V. Shlyapnikov and P. Pedri, Conference on correlated and Many-Body phenomena in Dipolar systems, Dresden, 2006.
- [30] S. Komineas and N.R. Cooper, *Phys. Rev. A* **75**, 023623 (2007).
- [31] H.-W. Hammer, A. Nogga, and A. Schwenk, *Rev. Mod. Phys.* **85**, 197 (2013).
- [32] D. S. Petrov, *Phys. Rev. Lett.* **112**, 103201 (2014).
- [33] A. Boudjemaa and G.V. Shlyapnikov, *Phys. Rev. A* **87**, 025601 (2013).
- [34] L.P. Pitaevskii, *JETP Letters* **40**, 511 (1984).
- [35] P. Nozieres, *J. Low Temp. Phys.* **137**, 45 (2004); *ibid.*, **142**, 91 (2006); *ibid.*, **156**, 9 (2009).
- [36] In the Supplemental Material available at <http://link.aps.org/supplemental...>, we present details of our numerical procedure and explicit expressions for $\mathcal{D}_{T(S)}(\theta)$, $\mathcal{C}_{T(S)}(\theta)$, $\mathcal{T}_{T(S)}(\theta)$.
- [37] L.D. Landau and E. M. Lifshitz, *Statistical Physics, Part 1* (Pergamon Press 1969).
- [38] K. Binder, *Rep. Prog. Phys.* **50**, 783 (1987).
- [39] In fact, one can think of the $g_2 = 0$ case as being represented by a vertical line in Fig.1 drawn at infinite $\tilde{\mu}$.
- [40] Such droplets have been discussed for 3D Bose condensates with contact two- and three-body interactions by A. Bulgac, *Phys. Rev. Lett.* **89**, 050402 (2002).
- [41] B. Spivak and S. A. Kivelson, *Phys. Rev. B* **70**, 155114 (2004).
- [42] S. Moroni and M. Boninsegni, *Phys. Rev. Lett.* **113**, 240407 (2014).

SUPPLEMENTARY MATERIAL

In the Supplemental Material we first derive explicit expressions for the energy functionals of the triangular and stripe supersolid states, in particular the expressions for the functions $\mathcal{C}_{T(S)}$, $\mathcal{D}_{T(S)}$, and $\mathcal{T}_{T(S)}$. The second part of the Supplemental Material is dedicated to the description of our numerical procedure of minimizing the grand potential density.

Derivation of the energy functionals for the triangular and stripe supersolid states

For calculating the energy functional we replace the field operators $\hat{\psi}(\mathbf{r})$ in the Hamiltonian (1) of the system with the condensate wavefunction $\psi_T(\mathbf{r})$ (7) for the triangular supersolid and with $\psi_S(\mathbf{r})$ (8) for the stripe phase. In both cases the kinetic energy term proves to be

$$\mathcal{K} = - \int d^2r \psi_{T(S)}^*(\mathbf{r}) \frac{\hbar^2 \nabla^2}{2m} \psi_{T(S)}(\mathbf{r}) = \frac{\hbar^2 k^2 n}{2m} \sin^2 \theta. \quad (12)$$

In the calculation of the contribution of the two-body interaction we use the effective momentum-dependent interaction amplitude of Eq.(2). Substituting this amplitude into equation (3) in which the field operators $\hat{\psi}(\mathbf{r})$ are replaced with the condensate wavefunction $\psi_{T(S)}(\mathbf{r})$ we obtain:

$$\mathcal{H}_2^{T(S)} = \mathcal{H}_{2c}^{T(S)} + \mathcal{H}_{2d}^{T(S)}, \quad (13)$$

$$\mathcal{H}_{2c}^{T(S)} = \frac{g_2}{2} \int d^2r |\psi_{T(S)}(\mathbf{r})|^4, \quad (14)$$

$$\mathcal{H}_{2d}^{T(S)} = \frac{1}{2} \int d^2r |\psi_{T(S)}(\mathbf{r})|^2 f(|\mathbf{r} - \mathbf{r}'|) |\psi_{T(S)}(\mathbf{r}')|^2, \quad (15)$$

where Eqs. (14) and (15) represent the contributions of the contact and dipole-dipole interactions, respectively, and the function $f(|\mathbf{r} - \mathbf{r}'|)$ writes:

$$f(|\mathbf{r} - \mathbf{r}'|) = -\pi d^2 \int \frac{d^2q}{(2\pi)^2} q \exp(i\mathbf{q}(\mathbf{r} - \mathbf{r}')). \quad (16)$$

The integration yields:

$$\mathcal{H}_{2c}^{T(S)} = g_2 n^2 \mathcal{C}_{T(S)}(\theta), \quad (17)$$

$$\mathcal{H}_{2d}^{T(S)} = -4\pi n^2 d^2 k \mathcal{D}_{T(S)}(\theta). \quad (18)$$

For the triangular phase the functions $\mathcal{C}_T(\theta)$ and $\mathcal{D}_T(\theta)$ are given by

$$\mathcal{C}_T(\theta) = \frac{1}{2} \left(\cos^4 \theta + 6 \cos^2 \theta \sin^2 \theta + 4\sqrt{\frac{2}{3}} \cos \theta \sin^3 \theta + \frac{5}{2} \sin^4 \theta \right), \quad (19)$$

$$\mathcal{D}_T(\theta) = \left[\cos^2 \theta + \sqrt{\frac{2}{3}} \cos \theta \sin \theta + \left(\frac{1}{4} + \frac{1}{2\sqrt{3}} \right) \sin^2 \theta \right], \quad (20)$$

and for the stripe phase we have:

$$\mathcal{C}_S(\theta) = \frac{1}{2} \left(1 + 4 \sin^2 \theta \cos^2 \theta + \frac{1}{2} \sin^4 \theta \right), \quad (21)$$

$$\mathcal{D}_S(\theta) = \left(1 - \frac{3}{4} \sin^2 \theta \right). \quad (22)$$

The integration of the third term of Eq.(1), representing the contribution of the three-body contact interaction,

$$\mathcal{H}_3^{T(S)} = \frac{g_3}{6} \int d^2r |\psi_{T(S)}(\mathbf{r})|^6, \quad (23)$$

leads to

$$\mathcal{H}_3^{T(S)} = g_3 n^3 \mathcal{T}_{T(S)}(\theta). \quad (24)$$

The expressions for the functions \mathcal{T}_T and \mathcal{T}_S read:

$$\mathcal{T}_T(\theta) = \frac{1}{6} \left(\cos^6 \theta + 15 \cos^4 \theta \sin^2 \theta + 20 \sqrt{\frac{2}{3}} \cos^3 \theta \sin^3 \theta + \frac{75}{2} \cos^2 \theta \sin^4 \theta + 30 \sqrt{\frac{2}{3}} \cos \theta \sin^5 \theta + \frac{85}{9} \sin^6 \theta \right). \quad (25)$$

$$\mathcal{T}_S(\theta) = \frac{1}{6} \left(1 + 12 \sin^2 \theta - \frac{9}{2} \sin^4 \theta - 6 \sin^6 \theta \right). \quad (26)$$

The summation of \mathcal{K} (12), \mathcal{H}_{2c}^i (17), \mathcal{H}_{2d}^i (18), and \mathcal{H}_3^i (24), where the symbol i stands for T and S , leads to the energy functional in the form (9).

Numerical procedure

The numerical calculation is performed in the grand canonical ensemble, with a given chemical potential μ and fixed volume of the system $V = L_x L_y$. The field operator $\hat{\psi}$ is treated as a classical field, and is discretized on a two-dimensional grid with periodic boundary conditions in the coordinate and momentum space. The grand potential reads:

$$\begin{aligned} \Omega[\psi^*, \psi] = & \int d^2 r \psi^*(\mathbf{r}) h_0 \psi(\mathbf{r}) + \frac{1}{2} \int d^2 r d^2 r' f(\mathbf{r} - \mathbf{r}') |\psi(\mathbf{r}')|^2 |\psi(\mathbf{r})|^2 \\ & + \frac{g_2}{2} \int d^2 r |\psi(\mathbf{r})|^4 + \frac{g_3}{6} \int d^2 r |\psi(\mathbf{r})|^6 - \mu \int d^2 r |\psi(\mathbf{r})|^2, \end{aligned} \quad (27)$$

where the single-particle Hamiltonian h_0 includes a possible presence of the harmonic trapping potential:

$$h_0 = -\frac{\hbar^2}{2m} \nabla^2 + \frac{1}{2} m \omega^2 r^2. \quad (28)$$

The number of grid points that we use along each direction ranges from 64 to 128 in the absence of the trapping potential and from 512 to 1024 in presence of an isotropic harmonic trap.

The ground state is determined by minimizing the grand potential (27) with the use of the *conjugate gradient* algorithm [1]. An ingredient of this method is the line minimization, that is in each iteration the wavefunction is changed as

$$\psi_{i+1}(\mathbf{r}) = \psi_i(\mathbf{r}) + \lambda \Delta \bar{\psi}_i(\mathbf{r}), \quad (29)$$

where $\psi_i(\mathbf{r})$ is the wavefunction in a current step, and λ is a real parameter chosen to minimize (27) along the proposed direction $\Delta \bar{\psi}_i(\mathbf{r})$. This procedure allows us to find the global minimum encountered when moving downhill in $\Omega[\psi^*, \psi]$ along a line. Consequently, it improves the efficiency of the calculation. The direction along which to move $\psi_i(\mathbf{r})$ is constructed as

$$\Delta \bar{\psi}_i(\mathbf{r}) = \Delta \psi_i(\mathbf{r}) + \frac{\int d^2 r \Delta \psi_i^*(\mathbf{r}) [\Delta \psi_i(\mathbf{r}) - \Delta \psi_{i-1}(\mathbf{r})]}{\int d^2 r |\Delta \psi_{i-1}(\mathbf{r})|^2} \Delta \bar{\psi}_{i-1}(\mathbf{r}), \quad (30)$$

in order to be *conjugate* with respect to the direction $\Delta \bar{\psi}_{i-1}(\mathbf{r})$ used in the previous step, and

$$\Delta \psi_i(\mathbf{r}) = -\frac{\delta \Omega}{\delta \psi^*} = -[\mathcal{H}_{\text{GP}}(\mathbf{r}) - \mu] \psi_i(\mathbf{r}), \quad (31)$$

is the gradient of the functional $\Omega[\psi^*, \psi]$ evaluated with $\psi_i(\mathbf{r})$, where

$$\mathcal{H}_{\text{GP}} = h_0 + \int d^2 r' f(\mathbf{r} - \mathbf{r}') |\psi(\mathbf{r}')|^2 + g_2 |\psi(\mathbf{r})|^2 + \frac{g_3}{2} |\psi(\mathbf{r})|^4 \quad (32)$$

is the Gross-Pitaevskii Hamiltonian. The integral in the second term of Eq. (32) can be calculated by using the convolution theorem [2], namely

$$\int d^2 r' f(\mathbf{r} - \mathbf{r}') |\psi(\mathbf{r}')|^2 = \mathcal{F}^{-1} \{ \mathcal{F}[f](\mathbf{q}) \mathcal{F}[|\psi|^2](\mathbf{q}) \} \quad (33)$$

where $\mathcal{F}[f](\mathbf{q})$ and $\mathcal{F}[|\psi|^2](\mathbf{q})$ are the Fourier transforms of $f(\mathbf{r})$ and $|\psi(\mathbf{r})|^2$ respectively, and \mathcal{F}^{-1} is the inverse transform. We set that the convergence is reached when the relative difference in the grand potential between the neighboring time steps is smaller than 5×10^{-9} .

In the absence of external trapping, the wave function can remain finite at the boundary. Due to the periodic boundary condition, the structure of the modulation for a non-uniform state is then limited by the size of the system imposed in the simulation. In order to overcome this constraint, for each given set of parameters (g_2, g_3, d, μ) we run the simulation several times with different L_x and L_y ranging from $4\pi/k_m$ to $9\pi/k_m$ respectively, where $k_m = 4\pi n r_* \mathcal{D}_{T(S)}(\theta)$ is fixed by the variational ansatz. In the end we choose the ground state as the one corresponding to the lowest grand potential density Ω/V .

Different trial wavefunctions are used in the simulation, including a uniform state, triangular (hexagonal) lattice state, square lattice state, stripe state, a combination of triangular (hexagonal) and stripe states. This is done in order to check whether the final result is biased by the initial conditions or not. We have also compared with each other the results obtained with a different number of grid points to make sure that they are not affected by the discretization of space.

-
- [1] W. H. Press, S. A. Teukolsky, W. T. Vetterling, and B. P. Flannery, *Numerical Recipes*, 3rd Edn. (Cambridge University Press 2007).
 [2] K. Góral and L. Santos, Phys. Rev. A **66**, 023613 (2002).
-